Original Article

MOLECULAR METABOLISM

Long non-coding RNA *LncCplx2* regulates glucose homeostasis and pancreatic β cell function

Linlin Wang [2,4,9], Liqiao Hu [2,9], Xingyue Wang [4,5,9], Zhaoxu Geng [4], Meng Wan [6], Junfeng Hao [6], Huisheng Liu [2,3], Yuying Fan [7,*], Tao Xu [2,3,4,8,], Zonghong Li [1,2,***]**

ABSTRACT

Objective: Numerous studies have highlighted the role of clock genes in diabetes disease and pancreatic β cell functions. However, whether rhythmic long non-coding RNAs involve in this process is unknown.

Methods: RNA-seq and 3' rapid amplification of cDNA ends (RACE)-PCR were used to identify the rat *LncCplx2* in pancreatic β cells. The subcellular analysis with qRT-PCR and RNA-Scope were used to assess the localization of *LncCplx2*. The effects of *LncCplx2* overexpression or knockout (KO) on the regulation of pancreatic β cell functions were assessed in vitro and in vivo. RNA-seq, immunoblotting (IB), Immunoprecipitation (IP), RNA pull-down, and chromatin immunoprecipitation (ChIP)-PCR assays were employed to explore the regulatory mechanisms through LncRNA-protein interaction. Metabolism cage was used to measure the circadian behaviors.

Results: We first demonstrate that *LncCplx2* is a conserved nuclear long non-coding RNA and enriched in pancreatic islets, which is driven by core clock transcription factor BMAL1. *LncCplx2* is downregulated in the diabetic islets and repressed by high glucose, which regulates the insulin secretion in vitro and ex vivo. Furthermore, *LncCplx2* KO mice exhibit diabetic phenotypes, such as high blood glucose and impaired glucose tolerance. Notably, *LncCplx2* deficiency has significant effects on circadian behavior, including prolonged period duration, decreased locomotor activity, and reduced metabolic rates. Mechanistically, *LncCplx2* recruits EZH2, a core subunit of polycomb repression complex 2 (PRC2), to the promoter of target genes, thereby silencing circadian gene expression, which leads to phase shifts and amplitude changes in insulin secretion and cell cycle genes.

Conclusions: Our results propose *LncCplx2* as an unanticipated transcriptional regulator in a circadian system and suggest a more integral mechanism for the coordination of circadian rhythms and glucose homeostasis.

Keywords LncCplx2; Glucose homeostasis; Pancreatic β cell; Insulin secretion

1. INTRODUCTION

Circadian rhythms adapt organisms to their daily surroundings in behavior and physiology. In mammals, circadian rhythms are driven by a web of cell-autonomous and self-sustained oscillators, which include the central oscillator within the suprachiasmatic nucleus (SCN) of the hypothalamus, and the peripheral oscillator present in nearly every cell of the body [1]. At the cellular level, the molecular mechanism responsible for driving the circadian oscillator comprises three interlocked transcriptional feedback loops [2]. The core components of circadian clock are the transcription factor CLOCK and its heterodimeric partner BMAL1, which binds to regulatory elements containing E-boxes [3]. In a secondary feedback loop, the BMAL1/CLOCK complex controls the rhythmic expression of nuclear receptors *REV-ERBα/β* and *RORα/β/r* [4]. In turn, REV-ERBα/β and RORα/β/r compete the ROR response elements (RORE) to control the expression of *BMAL1* and *NFIL3* [4]. The third BMAL1/CLOCK driven transcriptional loop involves D-box binding protein (DBP), thyrotroph embryonic factor (TEF), and

[1]The First Affiliated Hospital of Guangzhou Medical University, Guangzhou National Laboratory Clinical Base, Guangzhou Medical University, Guangzhou, China [2]Guangzhou National Laboratory, Guangzhou, China [3]School of Biomedical Engineering, Guangzhou Medical University, Guangzhou, China [4]National Laboratory of Biomacromolecules, CAS Center for Excellence in Biomacromolecules, Institute of Biophysics, Chinese Academy of Sciences, Beijing, China [5]Sino-Danish College, University of Chinese Academy of Sciences, Beijing, China [6]Core Facility for Protein Research, Institute of Biophysics, Chinese Academy of Science, Beijing, China [7]School of Life Sciences, Northeast Normal University, Changchun, China [8]Shandong First Medical University and Shandong Academy of Medical Sciences, Jinan, China

[9] These authors contributed equally to this paper.

*Corresponding author. School of Life Science, Northeast Normal University, Changchun, China. E-mail: fanyy033@nenu.edu.cn (Y. Fan).

**Corresponding author. Guangzhou National Laboratory, Guangzhou, China. E-mail: xutao@ibp.ac.cn (T. Xu).

***Corresponding author. The First Affiliated Hospital of Guangzhou Medical University, Guangzhou National Laboratory Clinical Base, Guangzhou Medical University, Guangzhou, China. E-mail: li_zonghong@gzlab.ac.cn (Z. Li).

Received September 19, 2023 • Revision received January 8, 2024 • Accepted January 9, 2024 • Available online 11 January 2024

https://doi.org/10.1016/j.molmet.2024.101878

hepatic leukemia factor (HLF), which interact with repressor nuclear factor interleukin-3 regulated protein (NFIL3) at D-box elements to fine-tune the circadian rhythms of *PER1/2* and *RORα/β/r* transcripts [5].
Numerous studies have revealed that islet clock genes play a central role in the control of insulin secretion and the development of diabetes [6,7]. For instance, studies performed in whole-body, pancreas-specific, and β cell-specific *Clock* or *Bmal1* knockout (KO) mice exhibit diabetic phenotypes, including hyperglycemia, hypoinsulinemic and impaired glucose tolerance [8—11]. The diabetic phenotypes are associated with impaired insulin secretion and β cell proliferation [10,11]. Consistent with these *in vivo* findings, *in vitro* or *ex vivo* experiments revealed that disturbed clock was sufficient to impair glucose-stimulated insulin secretion (GSIS) function in β cells [12,13]. The molecular mechanism underlying the circadian control of insulin secretion involves the binding of BMAL1/CLOCK complexes to distinct enhancers, which regulate time-dependent transcription of key exocytosis and metabolic genes in β cells [10]. In contrast to the hypoinsulinemic phenotype observed by *Bmal1* or *Clock* KO mice, the repressor gene period 2 (*Per2*) KO mice showed an enhanced GSIS function [14], and cryptochrome deficient (*Cry1* and *Cry2* double KO) mice were hyperinsulinemic [15].
LncRNA is considered as a class of non-coding RNAs without open reading frames, which is over 200 nt in length [16]. Recently, some small ORFs encoding functional micropeptides have been identified in LncRNAs [17]. Several studies identified groups of LncRNA showed circadian oscillations, which is under the control of circadian clock genes, and in turn, they have the potential impact on circadian biology or other specific function of tissues [18,19]. For example, a class of rhythmic LncRNAs, mostly regulated by BMAL1 and REV-ERBα, are involved in the metabolic homeostasis in the mouse liver [18,19]. In our previous study, we found a pancreatic islets enriched LncRNA antisense to *Cplx2*, namely *LncCplx2*, is downregulated in the islets of diabetic Goto-Kakizaki (GK) rats by RNA-seq analysis [20], as it was described in the atlas of circadian rhythmic LncRNAs in the rat pineal gland [21]. In this study, we found that *LncCplx2* regulates pancreatic β cell functions *in vitro* and *in vivo*. Mechanistically, *LncCplx2* recruits EZH2, a core subunit of PRC2, to the promoter of target genes, leading to suppress the circadian genes expression. Accordingly, *LncCplx2* deficiency causes overt diabetic phenotypes and disrupts circadian behaviors in mice.

2. MATERIALS AND METHODS

2.1. Cell culture

Min6 cells were cultured in Dulbecco's modified Eagle's medium (DMEM) medium containing 15% fetal bovine serum (FBS), 50 μM β-mercaptoethanol, 100 U/mL penicillin, and 100 μg/mL streptomycin. INS1 cells were cultured in RPMI 1640 medium containing 10% FBS, 1 mM sodium pyruvate, 50 μM β-mercaptoethanol, 100 U/mL penicillin, and 100 μg/mL streptomycin. Human Embryonic Kidney (HEK)-293T cells were cultured in DMEM medium containing 10% FBS, 100 U/mL penicillin, and 100 μg/mL streptomycin. All the cells were placed in a humidified atmosphere with 5% CO_2 at 37 °C.

2.2. Construction of *LncCplx2, Cplx2* or *Bmal1* KO cells and *LncCplx2*-rescued or overexpressed cells and *Bmal1* knockdown cells

LncCplx2, *Cplx2* or *Bmal1* KO Min6 cells were generated using CRISPR-Cas9. For *LncCplx2* KO cells, in order to avoid damaging the structure of the *Cplx2* gene, two sgRNAs were designed to cut out the second exon of *LncCplx2*, which account for the 90% of *LncCplx2* region. For *Cplx2* KO cells, two sgRNAs were designed to induce shift mutation of *Cplx2* gene reading frame, but not destruction of the *LncCplx2* transcript. For *Bmal1* KO cells, two sgRNAs were designed to induce shift mutation of *Bmal1* gene reading frame. One of the gRNAs was subcloned into the pLenti-CRISPR-V2 vector. The second gRNA was subcloned into a modified version of the pLenti-CRISPR-V2-BSD vector, in which the puromycin selection marker was substituted with a blasticidin selection marker. CRISPR plasmids were transiently transfected into HEK-293T cells together with pAdVAntage, VSVG and psPAX2 with a ratio 10:1.7:1:5. The HEK-293T culture media containing lentiviral particles were collected consecutively for two rounds and centrifuged in a Beckman SW 32 Ti rotor (Optima XPN-100) at 100,000 g for 1.5 h at 4 °C. Viral pellets were resuspended in PBS and used to infect target cells. Infected cells were sequentially selected using 1 μg/mL puromycin and 1 μg/mL blasticidin.
The *LncCplx2*-rescued cells or overexpressed cells were constructed with the lentiviral pLVX-IRES-Puro plasmid in *LncCplx2* KO Min6 cells or INS1 cells, respectively. Lentivirus was packaged by transfecting HEK-293T cells with pLVX-LncCplx2 plasmids and two packaging plasmids psPAX2 and VSVG with a ratio 4 : 3: 1. At 48 h posttransfection, the virus-containing supernatant was collected as above described, filtered and used to infect Min6 cells. The infected cells were selected and maintained with puromycin.
The Bmal1 knockdown Min6 cells was constructed with sh*Bmal1* plasmids. Briefly, 5 shRNA plasmids targeting different regions of *Bmal1* and a control shRNA plasmid (scrambled) were used to transfect Min6 cells with Lipofectamine 3000 (Invitrogen, L3000001), and positive cells were selected with G418 (Invitrogen, 11811023) for 2 weeks. qRT-PCR were used to determine the *Bmal1* expression level. The sequences of gRNA, shRNA are listed in Supplementary Table 3.

2.3. Animals

LncCplx2 KO mice were generated by GemPharmatech using the CRISPR-Cas9 system. Since the *LncCplx2* is an antisense RNA, in order to avoid damaging the structure of the *Cplx2* gene, the two sgRNAs were designed to cut out the second exon of *LncCplx2*, which account for the 90% of *LncCplx2* region. Cas9 mRNA and sgRNAs were co-injected into the fertilized eggs of C57BL/6JGpt mice. The fertilized eggs were transplanted to form positive F0 mice, which were confirmed by PCR and Sanger sequencing. A stable F1 generation mouse model was obtained by mating positive F0 generation mice with C57BL/6JGpt mice. Mice were housed in groups of three to five at 22—24 °C with a 12-h LD cycle. Animals had access to water ad libitum. All mice used in this study were gender- and age-matched. All animal experiments were approved by the Animal Care Committee at the Institute of Biophysics (License No. SYXK2021093).

2.4. Islet isolation

Pancreatic islets were isolated by collagenase digestion as described previously [20]. Briefly, the pancreas was inflated by instilling 5 mL of Hanks' buffered saline solution (HBSS) containing 0.5 mg/mL collagenase P through the pancreatic duct. The pancreas was harvested and incubated in a water bath at 37 °C for 25 min. The digested pancreas was rinsed with HBSS, and islets were separated on a Ficoll density gradient. After three washes with HBSS, the islets were manually isolated under a dissection microscope.

2.5. GSIS

Isolated islets were cultured in RPMI medium 1640 with 5.6 mM glucose for about 24 h. After washed with PBS, islets, Min6 or INS1

cells were pre-incubated for 1 h in 2.8 mM glucose Krebs–Ringer bicarbonate HEPES buffer (KRBB) containing: 114 mM NaCl, 4.7 mM KCl, 1.2 mM KH_2PO_4, 1.16 mM $MgSO_4$, 0.5 mM $MgCl_2$, 2.5 mM $CaCl_2$, and 20 mM HEPES with 0.2% BSA, pH 7.4. Next, groups of islets, Min6 or INS1 cells were batch-incubated in 0.2 mL, 2.8 mM glucose in KRBB for 1 h. Incubation medium was withdrawn for insulin measurement after gentle agitation and was replaced by 0.2 mL fresh KRBB solution supplemented with 16.8 mM glucose. For islets, all operations were conducted under dissection microscopy to avoid damaging the islets. Insulin was quantified by ELISA with commercially available kits.

2.6. Serum insulin measurements

For serum insulin detection, the mice were fasted for 12 h, then blood samples were collected into centrifuge tubes from the mouse orbital vein with no anti-coagulant. The clotted blood was centrifuged at 2,000 $\times$ *g* for 10 min to obtain serum. The supernatant serum was transferred into a clean tube and was analyzed using Rat/Mouse Insulin ELISA kit (Sigma-Aldrich, EZRMI-13K).

2.7. Glucose tolerance test

Glucose tolerance tests were performed in mice fasted for 12 h, blood glucose was measured after intra-peritoneal (i.p.) glucose injection of 2 g/kg body weight. Blood glucose was measured at 0, 15, 30, 60, and 120 min from tail vein blood samples.

2.8. Islet size measurements

Pancreases were dissected from paired WT and *LncCplx2* KO mice and fixed with 4% paraformaldehyde in PBS for 24 h. After dehydration, the samples were embedded in paraffin. We studied islet morphology for each section using H&E staining. 5 μm pancreas paraffin sections were deparaffinized and rehydrated before staining with hematoxylin solution for 5 min, followed by dips in 1% acid ethanol (1% HCl in 70% ethanol) and rinsed in distilled water. The sections were then stained with eosin for 3 min, dehydrated with graded alcohol and cleared in xylene. The sections were scanned with a Leica Aperio Versa 200 and Nikon DS-Ri2. Islet size and number of islets/mm^2 were analyzed by Fiji-ImageJ software.

2.9. Polysome profile

INS1 cells were treated with 100 μg/mL cycloheximide for 10 min at 37 °C, and digested by 0.05% trypsin–EDTA for 5 min and wash twice with cold PBS buffer. Lysis buffer composed with 15 mM Tris–HCl pH 7.4, 15 mM $MgCl_2$, 300 mM NaCl, 100 μg/mL cycloheximide, 1% Triton X-100, 40 U/μL RNAseOut and 24 U/mL DNAse was used to resuspend cells, and incubated on ice for 10 min, then centrifugated 5 min at 12,000 $\times$ *g* at 4 °C to remove nucleus. The supernatant was gently retrieved and floated on a 10–50% continuous sucrose gradient diluted with lysis buffer without NP40 in a SW40 tube. The samples were then centrifuged at 150,000 $\times$ *g* for 3 h at 4 °C. Sucrose gradient fractions were collected and concentrated by an equal volume of phenol-chloroform-isoamyl alcohol, followed by ethanol precipitation for the subsequent qRT-PCR analysis.

2.10. RNA-scope (RNA in situ hybridization)

The in situ hybridization was performed using the RNA-scope 2.5 HD Reagent Kit-BROWN (ACDBio, 322300) according to the manufacturers' instructions. The RNA-Scope probes were as follows: Mm-*LNCCPLX2*-01-C1 (ACDBio, 1090001) targeted *LncCplx2*, Negative Control Probe (ACDBio, 320871) and Positive Control Probe (ACDBio, 320881). The RNA fluorescence in situ hybridization was performed following protocol of RNA-scope Multiplex Fluorescent Regent Kit V2 (ACDBio, 323100) and RNA-Protein Co-Detection Ancillary Kit (ACDBio, 323180). *LncCplx2* probe co-labeled with two primary antibodies, insulin (Abcam, ab7842) and glucagon (Proteintech, 67286-1-Ig), with Opal fluorophores 520 Reagent (Akoya Biosciences, FP1487001KT) for glucagon, secondary antibody Rhodamine (TRITC) AffiniPure Goat Anti-Guinea Pig IgG (H + L) (Jackson IR, 106-025-003) for insulin, Opal fluorophores 650 Reagent (Akoya Biosciences, FP1496001KT) for *LncCplx2*. The mounted pancreas slices with DAPI were examined and photographed by Nikon DS-Ri2 and PerkinElmer Vectra 3 Automated Quantitative Pathology Imaging System.

2.11. RNA-seq

Total RNA was prepared with TRIzol regent (Invitrogen, 15596018) according to the manufacturer's instructions. Sequencing libraries were synthesized using the Hieff NGS Ultima Dual-Mode RNA Library Prep Kit for Illumina (YEASEN, 12252ES) according to the manufacturer's instructions. The libraries were sequenced on the Illumina NovaSeq 6000 PE150 (BerryGenomics). RNA raw sequence reads were aligned to the reference genome using STAR version 2.7.2b, and the raw and transcripts per million (TPM) count values were determined using RSEM version 1.3.3. Differentially expressed RNAs were identified by padj < 0.05 and $|\text{Log}_2 \text{ fold change}| > 2$ using DESeq2 version 1.32.0 in R 4.2.0. Interaction network were generated by the STRING database, confidence score was 0.7. The GO biological process enrichments were performed by clusterProfiler version 4.8.1 Raw mRNA sequence data have been deposited in the Genome Sequence Archive (https://ngdc.cncb.ac.cn/gsa) with accession number CRA008428.

2.12. Analysis of *LncCplx2* expression in islets of healthy and diabetic patients

The raw fastq files were downloaded from the European Nucleotide Archive (ENA) with the accession: PRJNA690574 (GEO: GSE164416). Raw sequence reads were aligned to the reference genome (hg38) using hisat2 version 2.2.0. Read count was calculated using htseq-count version 0.9.1 and the Gencode annotation file (v39). The read count of *LncCPLX2* were calculated using samtools, and TPM values were estimated with the consideration of total mapped reads and gene length. The BMI values of normal and diabetic group were kept within the same range of 28, and HbA1c values were less than 6 in the healthy group and more than 6 in the diabetic group (n = 18).

2.13. Metabolism cage

Mice were acclimated into CLAMS metabolic cage (Columbus Instruments) housing for one week before measurements were taken under a 12-h light–dark (LD) cycle. O_2 consumption, CO_2 production, energy expenditure, RER, feeding behavior and locomotor activity were measured with the CLAMS 6-chamber comprehensive monitoring system. Locomotor activity was determined as ambulatory counts when a series of infrared beams were interrupted sequentially on the horizontal X-axis/Y-axis (XAMB/YAMB), and feeding behavior was determined as ambulatory counts when a series of infrared beams were interrupted on the vertically (ZTOT).

To estimate the free running period of circadian rhythms, Chi-square periodogram analysis was applied for the free running period estimation, which was performed by calculating the Qp values of various possible periods [22]. The Qp values follow a probability distribution of $\chi 2$ when there are at least 10 cycles of circadian rhythm, and they were calculated by using the R package spectr [23,24]. The estimated period corresponding to the most significant Qp values was considered as the true free running period.

The active time was identified when the activity was equal to or greater than 10% mean activity of the top five peak activities on each day and at least 3 of the 6 following time points also met the criterion. And the main activity time was defined as between the first active time and the last active time during each day. The active onset and offset (min) were shown as the buffering time before the start of the main activity time or after the end of the main activity time which was caused by the delayed LD cycle. In-house developed R functions were used to analyze the activity data of mice, including the identification of active time and the calculation of activity onset and offset. The visualization of mice activity was performed with the R package ggplot2.

2.14. ChIP

ChIP-PCR was performed in Min6 cells or pancreatic islets using the Magnetic ChIP Kit (Pierce, 26157) according to the manufacturers' instructions. Briefly, Min6 cells or pancreatic islets were cross-linked by 1% formaldehyde (Invitrogen, 28908) for 10 min at room temperature, then quenched with glycine to a final concentration of 125 mM for 5 min. Sonication of cell lysis was performed by a ME220 Focused-ultrasonicator (Covaris). BMAL1 (Invitrogen, PA1-46118), E4BP4 (Proteintech, 11773-1-AP), NR1D1 (Proteintech, 14506-1-AP) and EZH2 (Invitrogen, 36—6300) antibody were used to pull down chromatin. Normal mouse/rabbit IgG or RNA Polymerase II antibodies (provided by ChIP kit) were used as the negative or positive control, respectively. ChIP-qPCR signals were calculated as fold enrichment of 1% input or non-specific antibody (isotype IgG antibodies) signals with at least two technical triplicates.

2.15. Luciferase reporter assay

LncCplx2 promoter region and a scrambled region were cloned into pGL6 luciferase vector. HEK-293T Cells were cotransfected with luciferase reporter, pRL-TK, and *Bmal1* overexpression plasmid. After 24-h transfection, cells were lysed and luciferase activities were determined using Dual-Luciferase Reporter Assay System and luminometer (BioTek SYNERGY NEO2). Firefly luciferase activity was normalized to renilla luciferase activity and expressed as relative luciferase unit.

2.16. RNA pull down

The *LncCplx2* was cloned into T7 promoter—based vector. The *LncCplx2* transcript and its antisense transcript were *in vitro* transcribed using biotin RNA labeling mix with T7 RNA polymerase or SP6 RNA polymerase. The mixtures were treated with RNase free DNase I and purified with TRIzol. Biotinylated RNAs were incubated with 20 μL of streptavidin C1 magnetic beads (Invitrogen, 65001) at room temperature for 30 min, and then incubated with nuclear proteins at 4 °C for 1 h. Proteins were eluted from the beads with elution buffer. The pulldown proteins were run on SDS-PAGE gels and followed IB analysis.

2.17. IP of RNP complexes

Pancreatic β cells were crosslinked with 1% formaldehyde and lysed in a buffer containing 20 mM Tris—HCl (pH 7.5), 100 mM KCl, 5 mM $MgCl_2$, 0.5% NP-40 and 1% proteinase inhibitor for 30 min on ice and centrifuged at 10,000 × *g* for 15 min at 4 °C. The supernatants were incubated with protein A/G magnetic beads (Thermo Fisher, 88802) coated with an anti-EZH2 antibody (Invitrogen, 36-6300) or control IgG (Invitrogen, 02-6102) overnight at 4 °C. Then, the beads were washed three times with wash buffer containing 50 mM Tris—HCl (pH 7.5), 150 mM NaCl, 1 mM $MgCl_2$ and 0.05% NP-40. The precipitates were incubated with 20 U of RNase-free DNase I for 15 min at 37 °C to remove DNA and were incubated further with 0.1% SDS/0.5 mg/mL Proteinase K at 55 °C for 15 min to remove proteins. The RNA isolated by IP was further analyzed by PCR.

2.18. 3′ RACE assay

3′ RACE was performed with Roche 3′ RACE kit (Roche, 3353621001) according to the manufacturer's instructions. RACE PCR productions were separated on a 1.5% agarose gel. Gel production were extracted with a Gel Extraction kit and sequenced.

2.19. qRT-PCR

Total RNA from GK rat islets, ob/ob and db/db mouse islets or cells was prepared with TRIzol regent according to the manufacturer's instructions, and then reverse transcribed by SuperQuick RT MasterMix. qRT-PCR was performed with cDNA (1:20 dilution), 2xSYBR Green PCR Mix, and specific primers (10 mM) listed in Supplementary Table S4 by QuantStudio 7 Flex Real-Time PCR Systems (Applied Biosystems). The 18S or *Gapdh* primers were used for normalization, and ΔCt was calculated to determine the relative expression levels.

2.20. IB

Whole-cell lysates prepared using RIPA buffer containing a proteinase inhibitor were separated by SDS-PAGE and transferred onto PVDF membranes. The membranes were incubated with primary antibodies against Tubulin (Proteintech, 66031-1-Ig), DDX1 (Proteintech, 11357-1-AP), SETD8 (Abcam, ab111691), HistoneH3 (Invitrogen, PA5-16183), CPLX2 (Proteintech, 18149-1-AP), BMAL1 (Invitrogen, PA1-46118), E4BP4 (Proteintech, 11773-1-AP), NR1D1 (Proteintech, 14506-1-AP), EZH2 (Invitrogen, 36-6300), and β-actin (Sigma Aldrich, A1978), followed by the appropriate HRP-conjugated secondary antibodies (Proteintech, SA00001-2/SA00001-1), and protein expression was detected with enhanced luminescence reagents (GE Healthcare, RPN2106).

2.21. Statistical analysis

All statistical analyses were acquired from more than two independent experiments, values were expressed as means ± SEM. Significance was calculated by two-tailed paired Student's t-test when two independent groups were compared. Two-way ANOVA was applied for multiple groups comparisons. *P*-value less than 0.05 was considered statistically significant. *$p < 0.05$, **$p < 0.01$, ***$p < 0.001$ and ****$p < 0.0001$. Statistical analyses were performed in GraphPad Prism 8.

3. RESULTS

3.1. *LncCplx2* is a conserved nuclear long non-coding RNA and enriched in pancreatic islets

Our previous study revealed a long non-coding RNA anti-sense *Cplx2*, termed *LncCplx2*, was downregulated in islets of diabetic Goto-Kakizaki (GK) rats by RNA-seq analysis [20]. Full-length RNA-seq and Poly A^+ 3′ end RNA-seq profiles indicated that *LncCplx2* was a short isoform with a different 3′ end terminal in pancreatic β cells (Figure S1a), which was confirmed by the 3′ rapid amplification of cDNA ends (RACE)-PCR (Figure S1b and Supplementary Table S1). RNA-seq analysis indicated that *LncCplx2* transcript was highly species-conservative in mice and humans (Figure S1c). *LncCplx2* showed the oscillatory expression pattern by serum shock in pancreatic β cells (Figure S1d), similar to the expression pattern described in the circadian rhythmic LncRNA atlas of the rat pineal gland [21]. The in silico and polysome profile results showed that

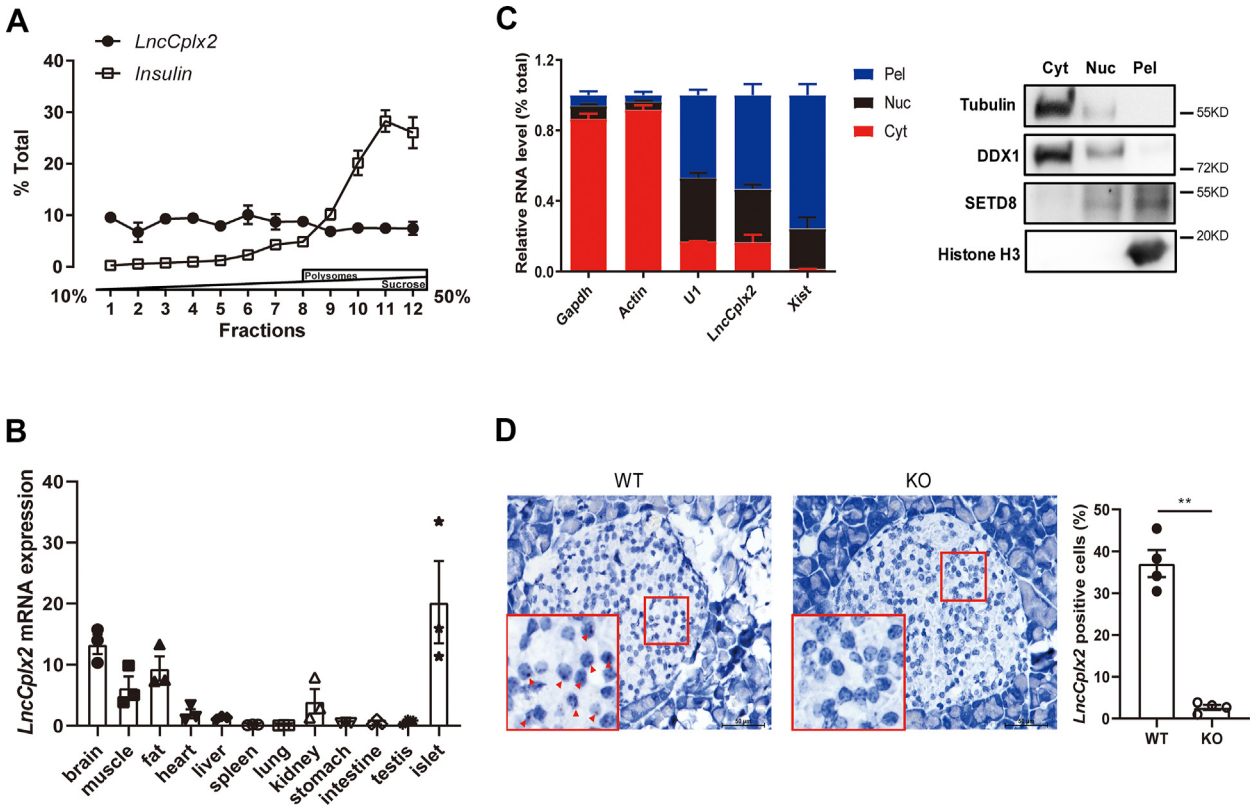

Figure 1: *LncCplx2* is a nuclear long non-coding RNA enriched in pancreatic islets. (A) Analysis of the relative distribution of *LncCplx2* and *Insulin* mRNA on polysome gradients in INS1 cells. (B) Analysis of *LncCplx2* expression by qRT-PCR in mouse tissues (n = 3). (C) Analysis of *LncCplx2* expression by qRT-PCR in INS1 cells following cell fractionation. The cytoplasm (Cyt), soluble nuclear (Nuc) and insoluble nuclear pellet (Pel) fractions were verified using specific markers through qRT-PCR and IB, respectively (n = 2). (D) RNA-scope images showing nuclear localization of *LncCplx2* in mouse islets. *LncCplx2* KO mouse islets were used as a negative control. Scale bar, 50 μm. The red arrowheads point the *LncCplx2* signals (n = 4). All the data are shown as the mean ± SEM. **p < 0.01, using two-tailed Student's t-test.

LncCplx2 was a non-coding transcript (Figures 1A, S1e and S1f). Further, a quantitative tissue distribution assay using qRT-PCR showed that *LncCplx2* was highly expressed in mouse pancreatic islets (Figure 1B). The subcellular analysis showed that the *LncCplx2* was almost located in the insoluble nuclear pellet along with the corresponding RNA and protein markers (Figure 1C). Consistently, RNA-Scope with H&E staining as well as staining of β cells and α cells showed that *LncCplx2* mainly located in the nucleus of β cells (Figures 1D and S1g). Intriguingly, *LncCplx2* was downregulated in the islets of diabetic GK rats, diabetic ob/ob and db/db mice, as well as diabetic patients (Figures S2a–d). Furthermore, *LncCplx2* expression was significantly repressed in INS1 and Min6 cells treatment with high glucose for 24 h and 48 h, respectively (Figures S2e–S2g). Collectively, *LncCplx2* is a conserved nuclear long non-coding RNA that is highly enriched in pancreatic islets and regulated by glucose.

3.2. *LncCplx2* regulates pancreatic β cell functions *in vitro* and *in vivo*

To explore the potential role of *LncCplx2* in regulating β cell function, we generated a *LncCplx2* KO Min6 cell line via the CRISPR-Cas9 technique. *LncCplx2 deficiency* significantly impaired the GSIS function of Min6 cells (Figure 2A). Notably, when *LncCplx2* expression was partially restored in the *LncCplx2* KO cells, GSIS function was also partially restored (Figure 2A). Consistently, overexpression of *LncCplx2* increased insulin secretion in INS1 cells (Figure 2B). These results suggest that *LncCplx2* plays a role in regulating insulin secretion *in vitro*. To verify whether *LncCplx2* also regulates insulin secretion *in vivo*, we generated whole body *LncCplx2* KO mice via the CRISPR-Cas9 technique with the same sgRNAs (Figure S3a–c). The *LncCplx2* KO mice showed efficient depletion of *LncCplx2* expression in pancreatic islets (Figures 1D and S3d). Consistently, insulin secretion was markedly impaired in *LncCplx2* KO islets compared to wild-type (WT) islets (Figure 2C). All these results suggest that *LncCplx2* regulates insulin secretion *in vitro* and *ex vivo*.

However, it was observed that the protein level of CPLX2 was significantly decreased in *LncCplx2* KO pancreatic islets and Min6 cells (Figure S4a and b). To rule out the possibility that the *LncCplx2*-deficient phenotypes was due to reduced CPLX2 protein levels. Firstly, we examined whether CPLX2 protein levels could be restored in *LncCplx2*-rescued cells. The results showed that CPLX2 protein levels remained unchanged (Figure S4b), while GSIS function could be partially rescued in the *LncCplx2*-rescued cells (Figure 2A), suggesting that the impaired insulin secretion was primarily due to *LncCplx2* deficiency rather than reduced CPLX2 protein levels. Furthermore, two *Cplx2* KO Min6 cell lines were generated using CRISPR-Cas9 to induce a shift mutation in the Cplx2 gene reading frame without disrupting the *LncCplx2* transcript (Figure S4c). The results showed that GSIS function was not changed after *Cplx2* deficiency (Figure S4d), indicating that other CPLX family proteins might compensate for CPLX2 deficiency. Indeed,

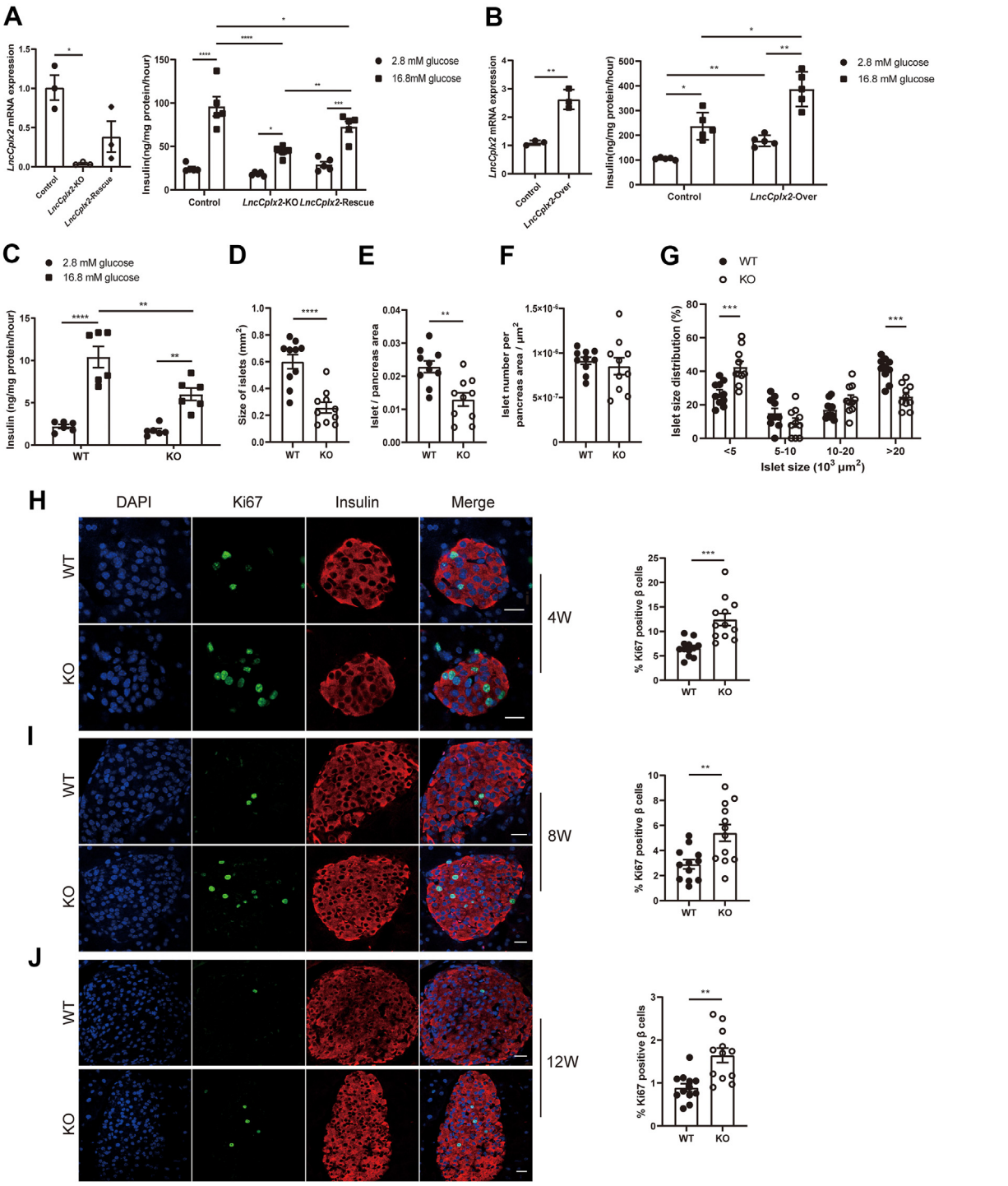

Figure 2: *LncCplx2* regulates pancreatic β cell function *in vitro* and *in vivo*. (A) GSIS in *LncCplx2* KO and *LncCplx2*-rescue Min6 cells compared to control cells (n = 5). (B) GSIS in *LncCplx2* overexpressed INS1 cells compared to control cells (n = 5). (C) GSIS in *ex vivo* islets isolated from WT and *LncCplx2* KO mice (n = 6, 12 weeks, male). (D–F) Comparison of size of islets (D), islet area per pancreas (E) and islet number per pancreas area (F) between WT and *LncCplx2* KO mice (n = 10, 12 weeks, male). (G) Distribution of different-sized islets in WT and *LncCplx2* KO mice (n = 10, 12 weeks, male). (H–J) Representative immunostaining of Ki67 for β cells (staining insulin) proliferation in WT and *LncCplx2* KO mice at 4 (H), 8 (I), and 12 (J) weeks (left). Scale bar, 10 μm. The quantitative analysis is shown in right panel (n = 12). All the data are shown as mean ± SEM. *p < 0.05, **p < 0.01, ***p < 0.001, ****p < 0.0001, using two-tailed Student's t-test and two-way ANOVA.

previous studies have shown that only the double KO of *Cplx1* and *Cplx2* resulted in decreased vesicle release in neuronal cells [15]. Taken together, these results showed that impaired insulin secretion is primarily caused by *LncCplx2* deficiency rather than reduced CPLX2 protein levels.

We next examined the morphology of pancreatic islets and found it to be comparable between age-matched WT and KO islets. However, quantification indicated that the islet size and islet size per pancreas area were significantly decreased in KO mice (Figure 2D and E). Interestingly, there was no significant change in the number of islets in

KO mice compared to WT littermates (Figure 2F), indicating that *LncCplx2* deficiency may affect islets proliferation. Furthermore, there was a significant reduction in the percentage of large islets and a significant increase in the percentage of small islets in KO mice compared to WT littermates (Figure 2G), which is consistent with the phenotypes observed in *Clock* or *Bmal1* KO mice [9]. To further confirm whether *LncCplx2* regulates islets proliferation, we performed the immunostaining Ki67 in *LncCplx2* deficient islets. The results showed that the Ki67 positive β cells were significantly increased in *LncCplx2* deficient islets (Figure 2H–J), suggesting that *LncCplx2* deficiency increases β cells proliferation. These findings indicate that *LncCplx2* deficiency also affects islet proliferation and mass.

3.3. *LncCplx2* regulates circadian clock genes expression

To elucidate the underlying mechanism by which *LncCplx2* regulates islet functions, a global transcriptome analysis was performed on isolated islets from WT and *LncCplx2* KO mice. A total of 374 differential expression genes (DEGs) were identified, of which 362 genes were up-regulated and 12 genes were down-regulated in the *LncCplx2* KO islets (Figure 3A, and Supplementary Table S2), indicating that *LncCplx2* is more likely to repress gene expression. Gene Ontology (GO) analysis showed significant enrichment in the process of MAPK signaling pathway, protein folding, rhythmic process and inflammatory response (Figure 3A). Intriguingly, STRING analysis showed that the interaction complexes were significantly enriched in rhythmic process, immediate-early gene, and chaperones-mediated autophagy (Figure 3B), which are known regulators of circadian rhythm. Examples of such genes include *Per1*, *Sik1*, and *Ciart*, which are core circadian transcription factors [25–27]. The AP-1 transcription factors *c-Fos*, *Fosb* and *Junb*, the zinc-finger protein *Egr3*, and the orphan receptor *Nr4a1*, are classic immediate-early genes that are important for light-induced phase-shifting of the circadian clock [28]. The *LncCplx2* deficient-induced chaperones, including *Dnajb1, Hsph1, Hspa1a*, and *Hspa1b*, are the components of the chaperone-mediated

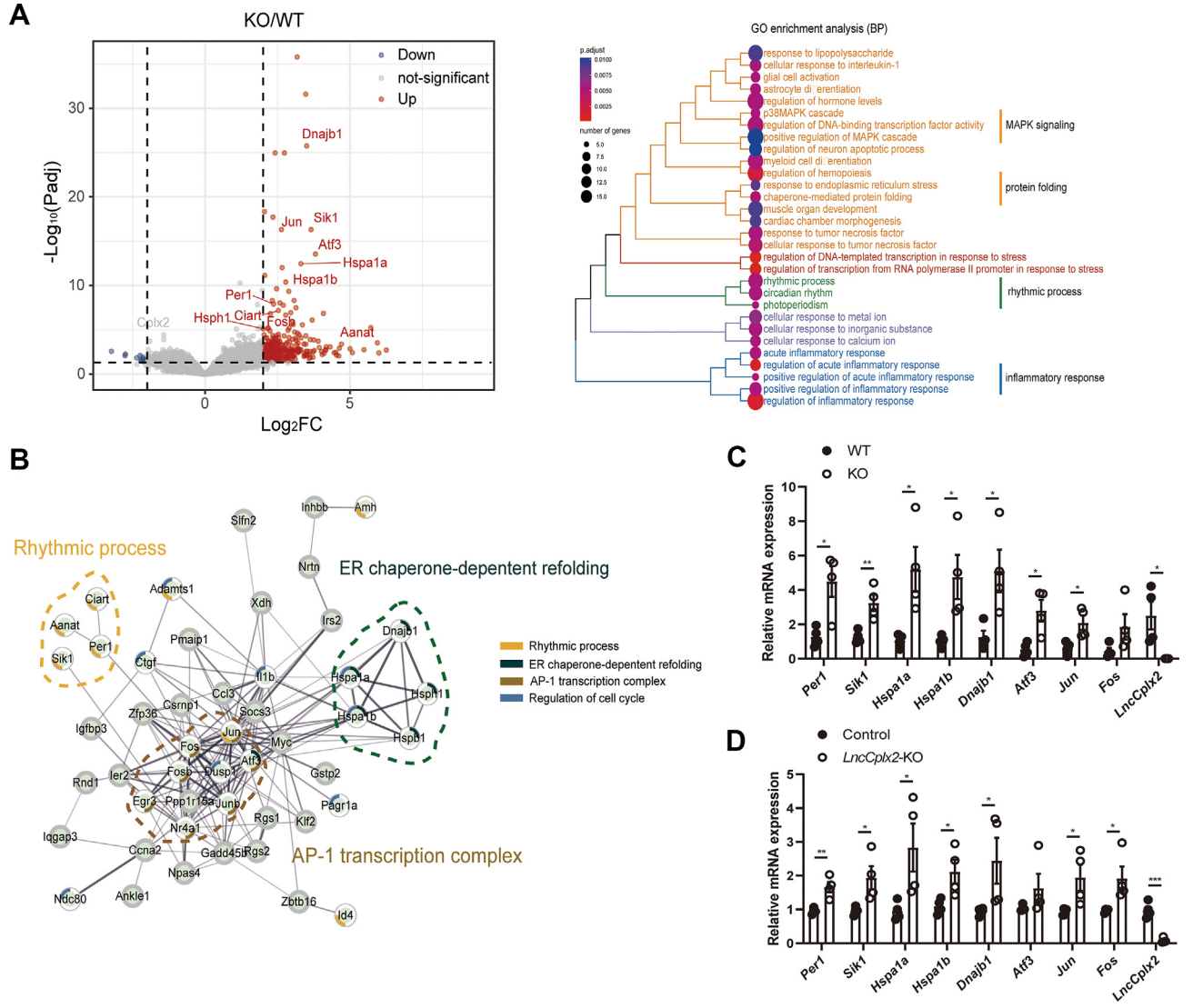

Figure 3: *LncCplx2* deficiency increases circadian gene expression. (A) Volcano plot (left) displaying RNA-seq analysis of islets from WT (n = 4) and *LncCplx2* KO mice (n = 4) at 16 weeks. DEGs (Log_2 Fold Change KO/WT >2 or <−2 with padj <0.05) are represented as red dots, with 362 genes upregulated and 12 genes downregulated. Gene Ontology (GO) analysis (right) of DEGs affected by *LncCplx2* deficiency. (B) Interaction network of DEGs based on the STRING database. Nodes are colored as indicated terms. (C–D) qRT-PCR analysis of DEGs in *LncCplx2* KO islets(c) (n = 4) and *LncCplx2* KO Min6 cells (D) (n = 4). All the data are shown as the mean ± SEM. *p < 0.05, **p < 0.01, ***p < 0.001, using two-tailed Student's t-test.

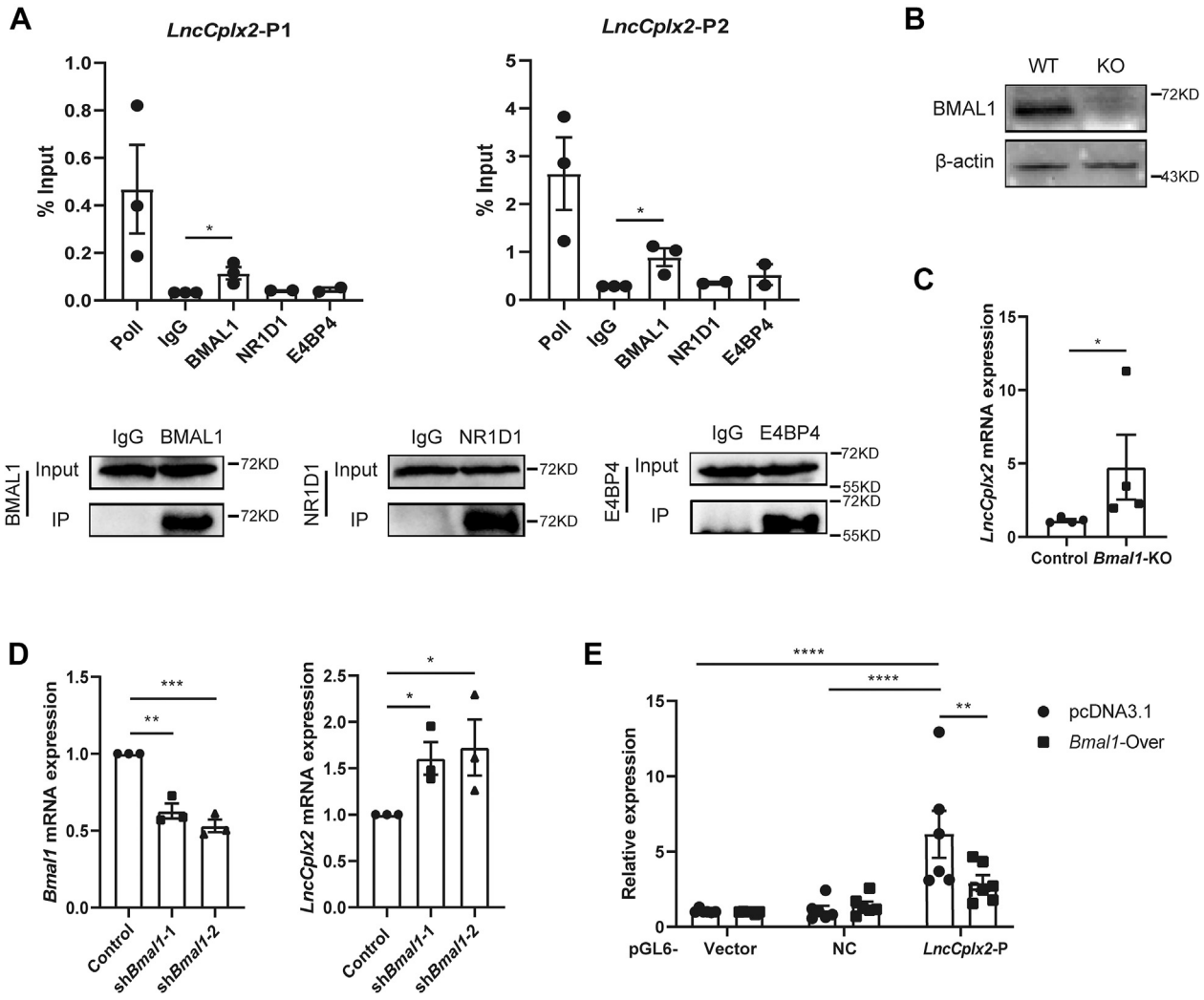

Figure 4: *LncCplx2* expression is regulated by BMAL1. (A) ChIP-qPCR assays demonstrating enrichment of BMAL1 at the *LncCplx2* promoter region in Min6 cells. RNA Polymerase II antibody and IgG serve as the positive and negative control, respectively (n = 3/2). Two different primer pairs (*LncCplx2*-P1 and *LncCplx2*-P2) targeted the promoter of LncCplx2 were used for the PCR assay. IB analysis of BMAL1, NR1D1 and E4BP4 antibody immunoprecipitation efficiency, IgG as negative control. (B) IB analysis of BMAL1 protein level in *Bmal1* KO and control Min6 cells. β-Actin was used as the loading control. (C) *LncCplx2* expression was analyzed by qRT-PCR in *Bmal1* KO and control Min6 cells (n = 4). (D) qRT-PCR analysis of *Bmal1* and *LncCplx2* expression in Min6 cells expressing two shRNAs targeting *Bmal1* and scrambled shRNA as control (n = 3). (E) Effects of *Bmal1* overexpression on different luciferase reporter activity driven by the *LncCplx2* promoter and negative control (n = 6). All the data are shown as the mean ± SEM. *p < 0.05, **p < 0.01, ***p < 0.001, ****p < 0.0001, using two-tailed Student's t-test and one-way ANOVA.

autophagy pathway, which contributes to the rhythmic removal of clock machinery proteins [29,30]. qRT-PCR results further confirmed the significant increase in the expression of several DEGs in *LncCplx2* KO pancreatic islets and Min6 cells (Figure 3C and D). Notably, no significant changes were observed in *Cplx2* KO cells (Figure S4e), suggesting that it is *LncCplx2*, rather than *Cplx2,* that regulates circadian gene expression.

It has been demonstrated that the molecular mechanism underlying circadian genes control of islet functions was through the regulation of time-dependent transcription of key exocytosis and metabolic genes in β cells [9,10,14]. We next sought to examine the differential rhythmic transcription of insulin secretion and cell cycle genes, every 4-h over a 24-h light–dark cycle by qRT-PCR in isolated islets from the WT and *LncCpx2* KO mice. As expected, all the examined genes showed circadian oscillations in the WT islets (Figure S5). Strikingly, *LncCplx2* deficiency significantly augmented the oscillatory amplitude of *InsR* (Figure S5). Conversely, the oscillatory amplitude of key β cell transcriptional factor *NeuroD1* was significantly decreased in the *LncCpx2* KO islets (Figure S5). In addition, the oscillatory amplitudes of *Ins1*, *Gck* and cyclinD1 were also changed but without statistical significance in the *LncCpx2* KO islets. Furthermore, *LncCplx2* deficiency leaded to the phase shift of transcriptional waves regarding insulin signaling genes (*Irs2*, *Akt2*, and *Pi3k*) (Figure S5). However, no significant change in oscillatory expression pattern of *Pdx1* was observed (Figure S5). Taken together, these results show that *LncCplx2* plays a role in modulating the rhythmic transcriptional waves of these genes, which are crucial for β cell function and insulin secretion.

3.4. *LncCplx2* expression is regulated by the clock transcription factor BMAL1

Circadian gene expression is generally driven by a transcriptional mechanism in which core clock genes act on three cis-elements (E-box, RORE, and D-box) in the target gene promoter region [2]. To

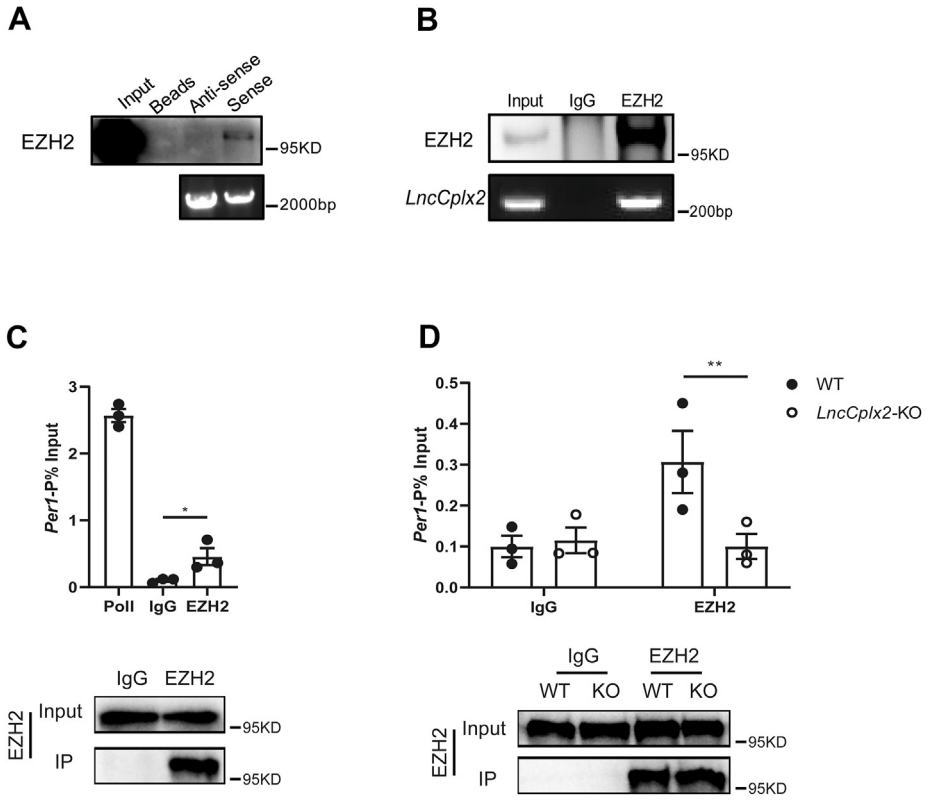

Figure 5: *LncCplx2* interacts with EZH2 to regulate gene expression. (A) IB analysis showing EZH2 pulled down by *LncCplx2* sense RNA transcript. Biotinylated *LncCplx2* was transcribed *in vitro*, and subjected to pull down interaction proteins, whereas antisense RNA served as the control. The *LncCplx2*-associated proteins captured by streptavidin beads were subjected to western blot analysis with specific anti-EZH2 antibody. Two independent experiments were performed. (B) RIP assays demonstrating that EZH2 could pull down the *LncCplx2* transcript. IB analysis of IP using an anti-EZH2 antibody, followed by RT-PCR analysis of the *LncCplx2* pulled down by the anti-EZH2 antibody. Two independent experiments were performed. (C) ChIP-qPCR assays showing enrichment of EZH2 at the *Per1* promoter region in Min6 cells (n = 3). IB analysis of EZH2 antibody immunoprecipitation efficiency, IgG as negative control. (D) ChIP-qPCR assays showing decreased enrichment of EZH2 at the *Per1* promoter region in *LncCplx2* KO islets compared to WT (n = 3). IB analysis of EZH2 antibody immunoprecipitation efficiency, IgG as negative control. All the data are shown as the mean ± SEM. *p < 0.05, **p < 0.01, using two-tailed Student's t-test.

investigate the potential transcriptional factor that directly regulates the *LncCplx2* expression, the chromatin immunoprecipitation (ChIP)-PCR assay was performed with specific antibodies targeting BMAL1, E4BP4 and NR1D1, which represent cis-acting proteins for E-box, RORE, and D-box, respectively. As a positive control, we found that the *LncCplx2* promoter region was significantly enriched by the anti-RNA Polymerase II (Pol II) antibody (Figure 4A), confirming the specificity of the assay. Strikingly, the *LncCplx2* promoter region could be enriched by the anti-BMAL1 antibody, but not by the anti-E4BP4 and anti-NR1D1 antibodies, compared to the enrichment attained by IgG (Figure 4A), implying that the expression of *LncCplx2* may be regulated by BMAL1. Consistently, the expression of *LncCplx2* was significantly increased in the *Bmal1* KO and knockdown Min6 cells (Figure 4B–D), supporting the notion that BMAL1 negatively regulates *LncCplx2* expression. Furthermore, we found a 1-kb *LncCplx2* promoter could increase the activity of luciferase reporter (Figure 4E). However, overexpression of *Bmal1* inhibited the activity of the luciferase reporter driven by a 1-kb *LncCplx2* promoter, but does not affect the activity of the luciferase reporter driven by a negative control and vector luciferase reporter (Figure 4E). Interestingly, *Bmal1* KO eliminated the high glucose-induced repression of *LncCplx2* expression, suggesting that high glucose downregulates *LncCplx2* through BMAL1 (Figure S2h). Taken together, these results suggest that BMAL1 regulates *LncCplx2* expression at the transcriptional level.

3.5. *LncCplx2* interacts with EZH2 to repress gene expression

To investigate the molecular mechanism underlying *LncCplx2* regulation of gene expression, we first explored the *LncCplx2*-interacting proteins using a pull-down assay. *LncCplx2* mainly represses gene expression, which promoted us to examine whether *LncCplx2* interacts with PRC2, a transcriptional repressor complex, to repress target gene expression [31]. RNA pull-down results showed that the core subunit of PRC2, EZH2, was pulled down by the *LncCplx2* transcript, but not by the control *LncCplx2* antisense transcript (Figure 5A). Conversely, RNA immunoprecipitation (RIP) results showed that *LncCplx2* transcript was significantly enriched by anti-EZH2 RIP compared to the enrichment attained by IgG RIP (Figure 5B). Taken together, these results indicate that *LncCplx2* interacts with EZH2. We sought to perform a ChIP assay to investigate the binding of EZH2 to the promoter region of *Per1*, one of the up-regulated DEGs in pancreatic islets due to *LncCplx2* deficiency. ChIP-PCR results indicated a significant enrichment of EZH2 to *Per1* promoter region (Figure 5C), consistent with previous results [32]. Strikingly, *LncCplx2* deficiency significantly decreased the enrichment of EZH2 to *Per1* promoter region (Figure 5D). Therefore, we speculate

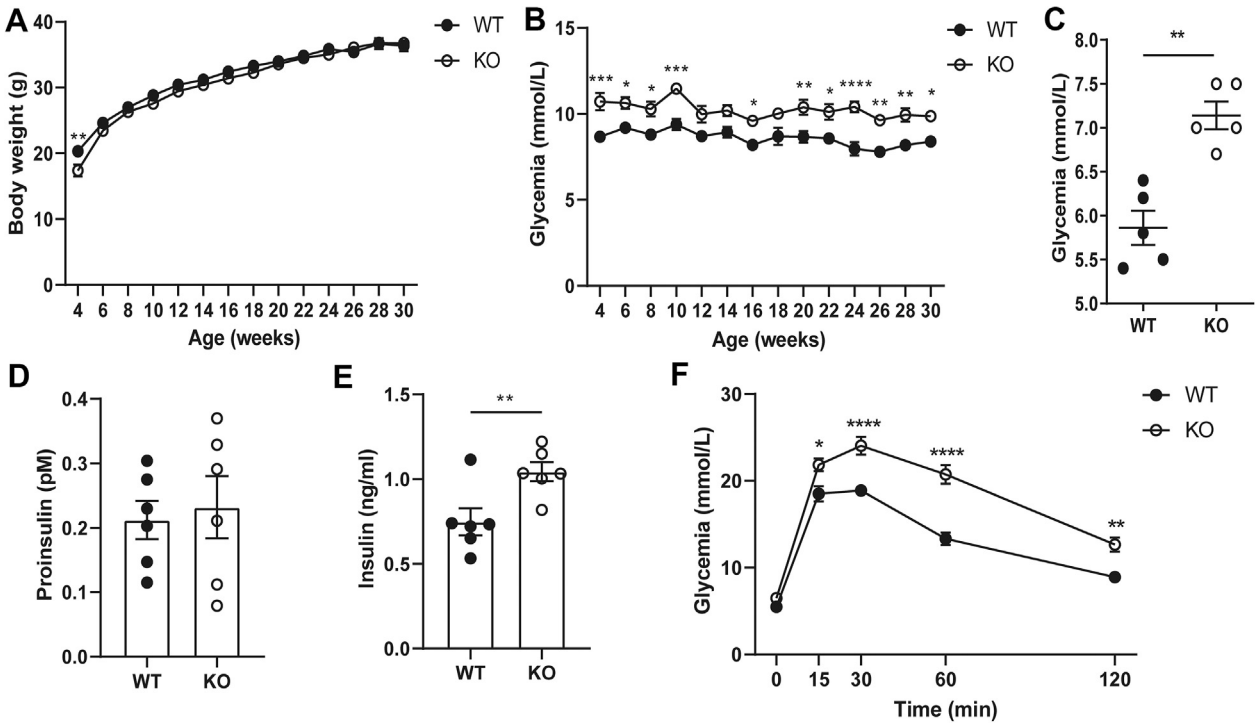

Figure 6: *LncCplx2*-deficient mice exhibit overt diabetic phenotypes. (A—B) Body weight (A) and random blood glucose (B) of WT and *LncCplx2* KO mice were measured from 4 weeks to 30 weeks (n = 8, male). (C—E) Fasted blood glucose (C), fasted proinsulin (D) and fasted insulin (E) of WT and *LncCplx2* KO mice was determined at 12 weeks (n = 5/6, male). (F) Blood glucose during glucose tolerance test (GTT) in WT and *LncCplx2* KO mice at 12 weeks (n = 12/10, male). All the data are shown as the mean ± SEM. *p < 0.05, **p < 0.01, ***p < 0.001, ****p < 0.0001, using two-tailed Student's t-test and two-way ANOVA.

that *LncCplx2* recruits EZH2 to the promoter of target genes, thereby silencing gene expression.

3.6. *LncCplx2* KO mice exhibit overt diabetic phenotypes

We went on to explore the physiological phenotypes of *LncCplx2* KO mice. The body weight of *LncCplx2* KO mice was reduced at 4 weeks old, compared with the WT mice (Figure 6A). However, no obvious phenotype with respect to body weight was observed from 6 weeks to study end (Figure 6A). Strikingly, the random blood glucose is increased from 4 weeks to study end in the *LncCplx2* KO mice (Figure 6B), suggesting that the *LncCplx2* deficiency disrupts glucose homeostasis. Consistently, *LncCplx2* KO mice exhibited high fasted blood glucose and insulin level, as well as normal fasted blood pro-insulin level, compared to WT mice (Figure 6C—E). Moreover, GTT result showed that *LncCplx2* deficiency significantly impaired glucose tolerance in mice (Figure 6F). Taken together, these results suggest that *LncCplx2* deficiency results in overt diabetic phenotypes.

3.7. *LncCplx2* KO mice disrupt circadian behaviors

Previous study showed that *LncCplx2* is a circadian rhythmic transcript in penal gland [21], which prompted us to examine whether *LncCplx2* deficiency could affect the circadian behaviors. Mice were placed in metabolic cages equipped with infrared sensors to detect locomotor activity under entrained 12-h of light and 12-h of dark cycle (LD). *LncCplx2* KO mice showed a slightly but significantly increased duration of the circadian period under entrained LD conditions (Figure 7A and B). Strikingly, the magnitude of locomotor activity was significantly decreased in the *LncCplx2* KO mice under entrained LD conditions (Figure 7C and D). Accordingly, the metabolic phenotypes showed that the *LncCplx2* KO mice exhibited less O_2 consumption, less CO_2 production and less energy expenditure, but normal respiratory exchange rate (RER), compared to WT mice (Figure 7E—H), consistent with the features of aging [29]. However, no obvious change in feeding behavior was observed between the WT and *LncCplx2* KO mice (Figure S6). Next, we examined the effects of *LncCplx2* deficiency on the synchronization of circadian rhythms using an experimental jet-lag model, in which mice were entrained in LD cycle for 10 days, then the LD cycles was delayed 6-h. The results showed that *LncCplx2* KO mice showed significantly faster re-entrainment compared to WT mice (Figure S7a and b). Consistently, the activity onset and offset of *LncCplx2* KO mice showed faster re-entrainment to the new LD cycle (Figure S7c and d). Taken together, these results show that *LncCplx2* deficiency disrupts the circadian behavior.

4. DISCUSSION

Overall, this study unveils an islets-enriched rhythmic long non-coding RNA *LncCplx2* plays a role in regulating glucose homeostasis and pancreatic β cell function by modulating circadian gene expression. The findings suggest that *LncCplx2* functions as an unexpected transcriptional regulator within the circadian system and provide insights into a more integrated mechanism for coordinating circadian rhythms and glucose homeostasis.

Numerous studies demonstrated that the circadian transcriptional loop is critical for maintenance of the glucose homeostasis [6,33]. Differential metabolic phenotypes were observed in various core clock gene mutant mice [33]. Both *Bmal1* KO or *Clock* mutant mice showed fasting hyperglycemia, impaired glucose tolerance and

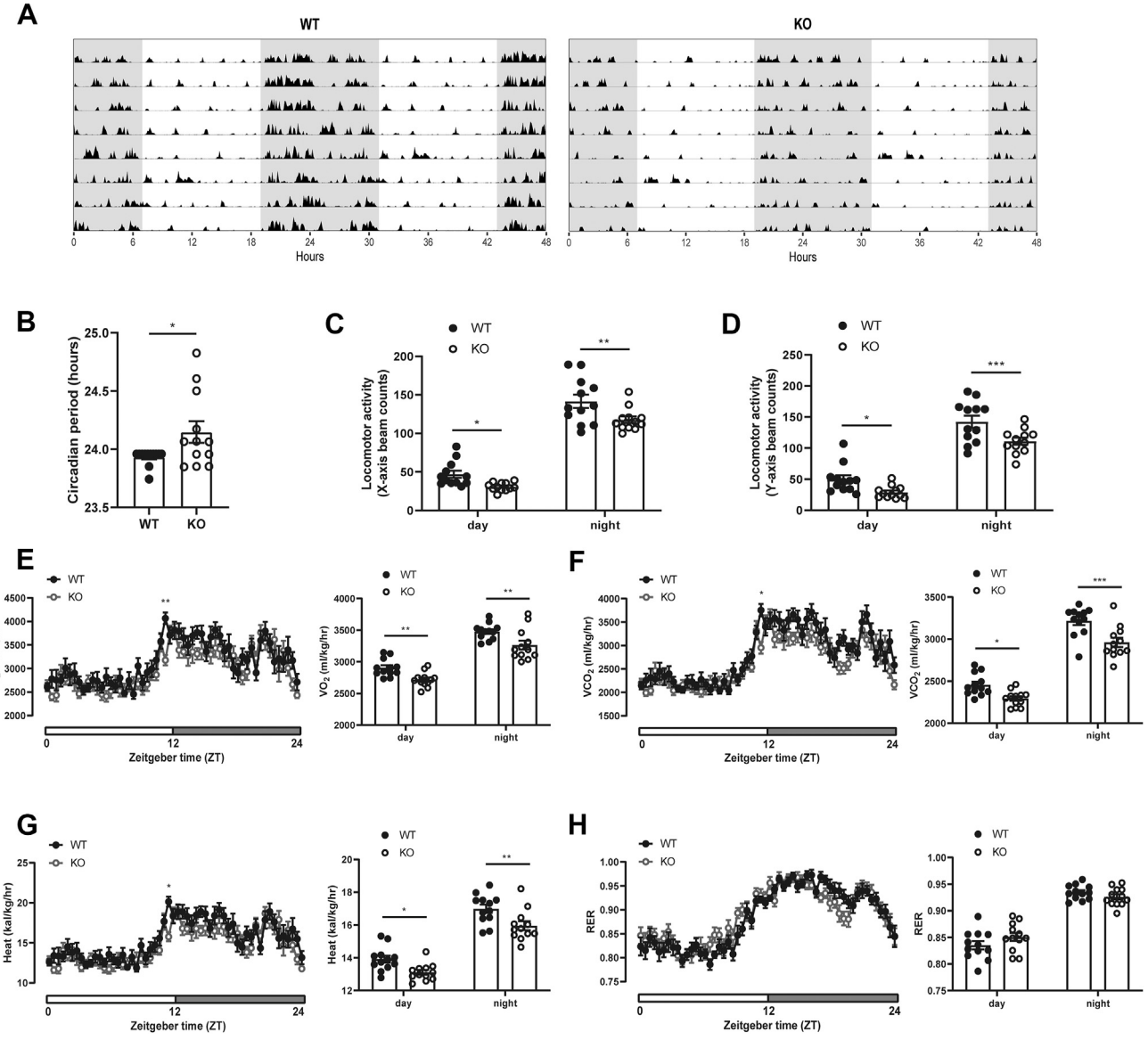

Figure 7: *LncCplx2* deficiency disrupts circadian behaviors. (A) Representative actogram of locomotor activity in WT and *LncCplx2* KO mice under an entrained LD cycle. (B) Circadian free running period in WT and *LncCplx2* KO mice under an entrained LD cycle (n = 12, 12 weeks, male). (C–D) Quantification of locomotor activities in the X-axis (C) and Y-axis (D) during the day or night time of WT and *LncCplx2* KO mice (n = 12, 12 weeks, male). (E–H), Average value of VO_2 (E), VCO_2 (F), HEAT (G) and RER (H) in WT and *LncCplx2* KO mice (n = 12, 12 weeks, male). All the data are shown as mean ± SEM. *p < 0.05, **p < 0.01, ***p < 0.001, using two-tailed Student's t-test and two-way ANOVA.

blunted insulin sensitivity [9]. Glucose homeostasis is also disrupted in the *Cry*-deficient or *Per*-deficient mice [14,15]. An overview of the metabolic disturbances reported for the different global clock gene KOs is well reviewed *en masse* [33]. In addition, it has been reported that the tissues-specific KO *Bmal1* or *Clock* is sufficient to disrupt the glucose homeostasis [9,10]. For example, the pancreas-specific and β cell-specific *Clock* or *Bmal1* KO mice exhibit diabetic phenotypes and disrupt the pancreatic β-cell function [10]. In this study, we found that *LncCplx2* deficiency exhibit the diabetic phenotypes, including hyperglycemia, impaired glucose tolerance, and defective in the pancreatic islets size and impaired GSIS function, consistent with the phenotypes of β-cell specific *Clock* or *Bmal1* KO mice. Furthermore, the molecular mechanism underlying BMAL1/CLOCK complexes circadian control of glucose homeostasis has been demonstrated to be through the regulation of time-dependent transcription of key β cell exocytosis, proliferation and metabolic genes [10]. Consistently, *LncCplx2* deficiency leads to the phase shifts and amplitude changes of clock-dependent transcriptional waves of insulin signaling and cell cycle genes, indicating that the molecular mechanism underlying *LncCplx2* affect the pancreatic islet function is through the regulation of circadian gene expression. This study has shed new light into the fascinating connection between circadian rhythm and metabolism.

AUTHOR CONTRIBUTIONS

T.X. and Z.L. conceived the project. L.W., T.X. and Z.L. prepared the manuscript. L.W. and Z.L. contributed to the experiments design, data

acquisition and analysis. L.W. carried out animal experiments. L.H. and X.W. performed bioinformatics analysis. Z.G. help with RNA-seq analysis. M.W. and J.H. performed the RNA in situ hybridization. Y.F. help review and edit the manuscript. All the authors discussed the data and reviewed the manuscript. Z.L. contributed to the study conceptualization, resources, investigation, review and editing of the manuscript, supervision, project administration, and funding acquisition, and is the guarantor and takes full responsibility for the work as a whole, including the study design, access to data, and the decision to submit and publish the manuscript.

ACKNOWLEDGMENTS

We thank the staff of the Institute of Biophysics Core Facilities, in particular, Zhenwei Yang for technical support with qRT-PCR and Zheng Liu for technical support with mouse feeding. This work was supported by grants from the National Natural Science Foundation of China (82200884 to Z.L. and 31730054 to T.X.), National Key Research and Development Program (2021YFA1300301 to T.X.) and Guangdong Province High-level Talent Youth Project (2021QN02Y939 to Z.L.).

DECLARATION OF COMPETING INTEREST

The authors declare no competing interests.

DATA AVAILABILITY

Data will be made available on request.

APPENDIX A. SUPPLEMENTARY DATA

Supplementary data to this article can be found online at https://doi.org/10.1016/j.molmet.2024.101878.

REFERENCES

[1] Hastings MH, Reddy AB, Maywood ES. A clockwork web: circadian timing in brain and periphery, in health and disease. Nat Rev Neurosci 2003;4:649–61.
[2] Takahashi JS. Transcriptional architecture of the mammalian circadian clock. Nat Rev Genet 2017;18:164–79.
[3] Shearman LP, Sriram S, Weaver DR, Maywood ES, Chaves I, Zheng B, et al. Interacting molecular loops in the mammalian circadian clock. Science 2000;288:1013–9.
[4] Preitner N, Damiola F, Lopez-Molina L, Zakany J, Duboule D, Albrecht U, et al. The orphan nuclear receptor REV-ERBalpha controls circadian transcription within the positive limb of the mammalian circadian oscillator. Cell 2002;110:251–60.
[5] Mitsui S, Yamaguchi S, Matsuo T, Ishida Y, Okamura H. Antagonistic role of E4BP4 and PAR proteins in the circadian oscillatory mechanism. Genes Dev 2001;15:995–1006.
[6] Vieira E, Burris TP, Quesada I. Clock genes, pancreatic function, and diabetes. Trends Mol Med 2014;20:685–93.
[7] Lee J, Liu R, de Jesus D, Kim BS, Ma K, Moulik M, et al. Circadian control of beta-cell function and stress responses. Diabetes Obes Metab 2015;17(Suppl 1):123–33.
[8] Rudic RD, McNamara P, Curtis AM, Boston RC, Panda S, Hogenesch JB, et al. BMAL1 and CLOCK, two essential components of the circadian clock, are involved in glucose homeostasis. PLoS Biol 2004;2:e377.
[9] Marcheva B, Ramsey KM, Buhr ED, Kobayashi Y, Su H, Ko CH, et al. Disruption of the clock components CLOCK and BMAL1 leads to hypoinsulinaemia and diabetes. Nature 2010;466:627–31.
[10] Perelis M, Marcheva B, Ramsey KM, Schipma MJ, Hutchison AL, Taguchi A, et al. Pancreatic beta cell enhancers regulate rhythmic transcription of genes controlling insulin secretion. Science 2015;350:aac4250.
[11] Sadacca LA, Lamia KA, deLemos AS, Blum B, Weitz CJ. An intrinsic circadian clock of the pancreas is required for normal insulin release and glucose homeostasis in mice. Diabetologia 2011;54:120–4.
[12] Vieira E, Marroqui L, Batista TM, Caballero-Garrido E, Carneiro EM, Boschero AC, et al. The clock gene Rev-erbalpha regulates pancreatic beta-cell function: modulation by leptin and high-fat diet. Endocrinology 2012;153:592–601.
[13] Marcheva B, Ramsey KM, Bass J. Circadian genes and insulin exocytosis. Cell Logist 2011;1:32–6.
[14] Zhao Y, Zhang Y, Zhou M, Wang S, Hua Z, Zhang J. Loss of mPer2 increases plasma insulin levels by enhanced glucose-stimulated insulin secretion and impaired insulin clearance in mice. FEBS Lett 2012;586:1306–11.
[15] Barclay JL, Shostak A, Leliavski A, Tsang AH, Johren O, Muller-Fielitz H, et al. High-fat diet-induced hyperinsulinemia and tissue-specific insulin resistance in Cry-deficient mice. Am J Physiol Endocrinol Metab 2013;304:E1053–63.
[16] Yao RW, Wang Y, Chen LL. Cellular functions of long noncoding RNAs. Nat Cell Biol 2019;21:542–51.
[17] Patraquim P, Magny EG, Pueyo JI, Platero AI, Couso JP. Translation and natural selection of micropeptides from long non-canonical RNAs. Nat Commun 2022;13:6515.
[18] Fan Z, Zhao M, Joshi PD, Li P, Zhang Y, Guo W, et al. A class of circadian long non-coding RNAs mark enhancers modulating long-range circadian gene regulation. Nucleic Acids Res 2017;45:5720–38.
[19] Vollmers C, Schmitz RJ, Nathanson J, Yeo G, Ecker JR, Panda S. Circadian oscillations of protein-coding and regulatory RNAs in a highly dynamic mammalian liver epigenome. Cell Metab 2012;16:833–45.
[20] Hou J, Li Z, Zhong W, Hao Q, Lei L, Wang L, et al. Temporal transcriptomic and proteomic landscapes of deteriorating pancreatic islets in type 2 diabetic rats. Diabetes 2017;66:2188–200.
[21] Coon SL, Munson PJ, Cherukuri PF, Sugden D, Rath MF, Moller M, et al. Circadian changes in long noncoding RNAs in the pineal gland. Proc Natl Acad Sci U S A 2012;109:13319–24.
[22] Sokolove PG, Bushell WN. The chi square periodogram: its utility for analysis of circadian rhythms. J Theor Biol 1978;72:131–60.
[23] Refinetti R, Lissen GC, Halberg F. Procedures for numerical analysis of circadian rhythms. Biol Rhythm Res 2007;38:275–325.
[24] Hughey J, Tackenberg M. ectr: Calculate the Periodogram of a Time-Course. Version 1.0.1 2022. Available from: https://github.com/hugheylab/spectr.
[25] Jagannath A, Butler R, Godinho SIH, Couch Y, Brown LA, Vasudevan SR, et al. The CRTC1-SIK1 pathway regulates entrainment of the circadian clock. Cell 2013;154:1100–11.
[26] Numano R, Yamazaki S, Umeda N, Samura T, Sujino M, Takahashi R, et al. Constitutive expression of the Period1 gene impairs behavioral and molecular circadian rhythms. Proc Natl Acad Sci U S A 2006;103:3716–21.
[27] Annayev Y, Adar S, Chiou YY, Lieb JD, Sancar A, Ye R. Gene model 129 (Gm129) encodes a novel transcriptional repressor that modulates circadian gene expression. J Biol Chem 2014;289:5013–24.
[28] Morris ME, Viswanathan N, Kuhlman S, Davis FC, Weitz CJ. A screen for genes induced in the suprachiasmatic nucleus by light. Science 1998;279:1544–7.
[29] Juste YR, Kaushik S, Bourdenx M, Aflakpui R, Bandyopadhyay S, Garcia F, et al. Reciprocal regulation of chaperone-mediated autophagy and the circadian clock. Nat Cell Biol 2021;23:1255–70.
[30] Agarraberes FA, Dice JF. A molecular chaperone complex at the lysosomal membrane is required for protein translocation. J Cell Sci 2001;114:2491–9.

[31] Long Y, Hwang T, Gooding AR, Goodrich KJ, Rinn JL, Cech TR. RNA is essential for PRC2 chromatin occupancy and function in human pluripotent stem cells. Nat Genet 2020;52:931–8.

[32] Etchegaray JP, Yang X, DeBruyne JP, Peters A, Weaver DR, Jenuwein T, et al. The polycomb group protein EZH2 is required for mammalian circadian clock function. J Biol Chem 2006;281:21209–15.

[33] Kalsbeek A, la Fleur S, Fliers E. Circadian control of glucose metabolism. Mol Metab 2014;3:372–83.

[34] Moran I, Akerman I, van de Bunt M, Xie R, Benazra M, Nammo T, et al. Human beta cell transcriptome analysis uncovers lncRNAs that are tissue-specific, dynamically regulated, and abnormally expressed in type 2 diabetes. Cell Metab 2012;16:435–48.

